POAC'25
St. John's, Newfoundland and Labrador, Canada

Proceedings of the 28th International Conference on Port and Ocean Engineering under Arctic Conditions
Jul 13-17, 2025
St. John's, Newfoundland and Labrador
Canada

Model testing and analytical research on ice breaking resistance of a segemented ship bow

Gang Xuhao, Tian Yukui*, Yu Chaoge, Ji Shaopeng, Kong Shuai, Kou Ying
China Ship Science Research Center, National Key Laboratory of Hydrodynamics
Wuxi 214082, China
(*correspondence: tianyukui@cssrc.com.cn)

ABSTRACT

Ice resistance prediction of ships navigating in ice is the focus of navigation performance prediction, and clarifying the formation mechanism and composition of ice breaking resistance is an essential means to improve the accuracy of this prediction. In this paper, a bow model was designed, and the model tests in level ice, pre-sawn ice and open water were carried out in the small ice model basin of China Ship Science Research Center (CSSRC SIMB). The ice breaking process, ice fracture phenomenon and ice breaking resistance components were observed and quantified. And, with the tests implemented, a dimensionless analysis of the bow resistance components was performed, and the non-dimensional coefficients for ice resistance terms were derived, enabling the establishment of a predictive equation for total ice resistance. The findings offer valuable insights for engineering applications, particularly in ice resistance prediction, resistance component identification, and ship design optimization.

KEY WORDS: Ice breaking; Model test; Resistance decomposition; Dimensionless analysis; Ice resistance prediction

INTRODUCTION

With global climate warming, arctic ice coverage has been retreating rapidly, unveiling abundant natural resources and navigational opportunities. Ice-going vessels have become indispensable for exploiting these resources. Ice resistance poses a significant challenge in ship design and operation, directly impacting operational efficiency and safety. Consequently, accurate simulation of the ice-breaking process and reliable forecasting of ice resistance are of paramount theoretical and practical importance.

Conducting model experiments in ice basin, with precise control of experimental parameters to simulate real ice conditions and ship icebreaking scenarios, can profoundly reveal the intrinsic relationships among various physical phenomena and determine both icebreaking resistance and overall ice resistance, thereby possessing extremely important engineering application value. Through detailed research, Valanto (2001) divided the bow icebreaking process into three stages: fracturing failure, rotational immersion, and slippage clearance, thus simplifying the ship-ice interaction process. Based on numerous model test results from the Canadian NRCC-IOT ice basin, Spencer (2001) decomposed ice resistance into several

components and proposed an empirical method for calculating ice resistance. Jeong et al. (2010) in Korea Research Institute of Ships and Ocean Engineering (KRISO) ice basin, conducted icebreaking tests under multi-level ice conditions to study the components of ice resistance and, on basis of Spencer's research, obtained empirical formulas for predicting ice resistance. Daniela Myland (2016) in HSVA conducted icebreaking experiments using ship models with different bow geometries to investigate the influence of bow shape on ice resistance. Furthermore, Daniela Myland employed the DTMAB5415 model to detach the model bow from the overall model and reassemble it using sensors and other devices, successfully achieved the decomposition of bow resistance from other resistive forces during the icebreaking process.

Despite these advances, most studies have relied on broad categorizations of ice resistance rather than detailed component measurements. This study addresses this gap by designing a systematic methodology for measuring ice resistance components in the small ice model basin of China Ship Science Research Center (CSSRC SIMB). The ice resistance components were directly measured, and each resistance component was analyzed using dimensionless analysis. By combining these non-dimensional analyses applied to test data, a suitable dimensionless expression method for ice resistance obtained in the ice basin was developed.

EXPERIMENTAL DESIGN FOR ICE RESISTANCE ANALYSIS

CSSRC Small Ice Model Basin

The small ice model basin in China Ship Scientific Research Center (CSSRC SIMB) measures 8 m in length, 2 m in width, and 1 m in depth. Fig. 1 depicts the interior of the ice water basin. The columnar model ice utilized in the experiments was fabricated from a sodium chloride solution through controlled freezing processes. Initially, the saline mixture was cooled to near its freezing point to perform crystal seeding. Subsequently, under conditions of approximately -20 °C, the mixture was gradually frozen to form an ice layer containing brine pockets. After achieving the desired thickness, the ice layer's strength was adjusted through warming up. Once the target strength was attained, the temperature was maintained constant, and the experimental tests were initiated.

Figure 1. Interior of CSSRC SIMB

Design of Test Model

Icebreaker bows differ markedly from conventional ship bows, and various types of icebreaker bows exhibit distinct performance characteristics in icebreaking operations.

To measure the total ice resistance and its individual components during the ship – ice interaction, and to investigate the roles of these resistance components and their relationship

with overall ice resistance, a simplified Waas bow was selected. The basic parameter of the model can be found in Table1. And three force-measuring segments were strategically placed along the starboard side (Fig. 2).

Table 1 Basic parameters of the bow model

Parameter	Suit	Value
Displacement	m^3	0.12
Bow length	m	0.96
Width of bow front	m	0.40
Width of bow rear	m	0.46
Draught	m	0.18
Bow angle	°	24
Entrance angle	°	84
Flat angle	°	52

On the starboard side of the bow model, the first segment is located near the waterline (ice surface) and serves as the primary sensor for icebreaking forces, as it directly contacts and penetrates the ice sheet during icebreaking. The second segment follows closely behind, situated beneath the bow's inclined section below the waterline, and measures the forces resulting from fractured ice fragments sliding along the hull surface. The third segment is positioned at the bow's bottom, connecting to the parallel section, and detects the forces caused by ice fragments sliding onto the hull bottom due to buoyancy. Each segment is connected to the model via a force measurement system, with gaps maintained between the segments and between the segments and the main hull to ensure that force measurements are not interfered.

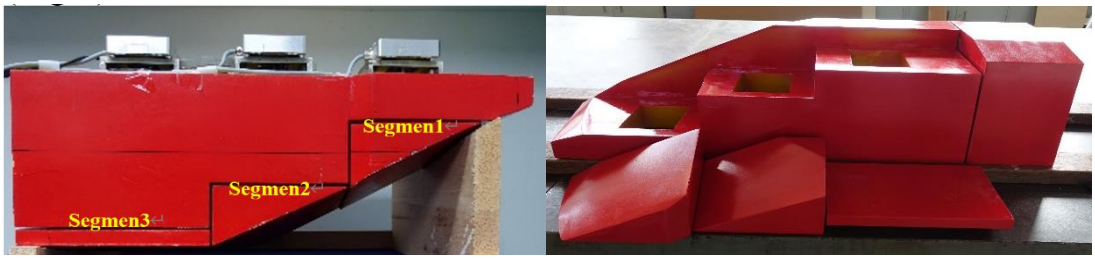

Figure 2. Ship model and segment diagram

In order to investigate the relationship between total ice resistance and its constituent components, the total ice resistance of the bow model and each segment was measured. A six-component force sensor was employed to capture the overall ice resistance experienced by the bow. Additionally, three-component force sensors were utilized to measure the forces acting on each segment. The total force sensor was mounted on the upper surface, positioned directly above the center of mass of the bow model, while the segment force sensors were affixed to the bottoms of the segments and connected to the main hull through rods (Fig. 3). Furthermore, three underwater video cameras were evenly distributed and fixed at the bottom of the ice tank to observe the interaction between the bow and the ice as well as the movement of ice floes.

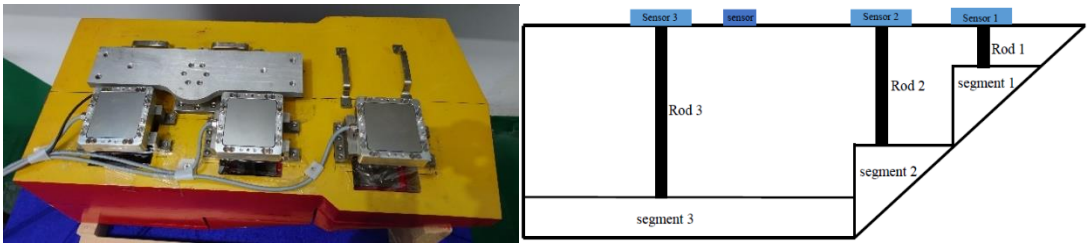

Figure 3. Measurement Setup

Test Methodology and Conditions

To decompose the total ice resistance of the bow model and extract the ice-breaking resistance, the ice resistance test method of ITTC was referenced. Level ice tests and pre-sawn ice tests were conducted in the CSSRC ice basin at ice-breaking speeds of 0.01 m/s, 0.05 m/s, 0.10 m/s, 0.15 m/s, and 0.20 m/s. During the ship bow ice-breaking resistance tests, the towing carriage and the ship bow model were rigidly connected via a strut. The heave and pitch of the model were not considered during the tests, and the model was towed in a constrained condition and a constant velocity was maintained.

Figure 4. Level ice tests and pre-sawn ice tests

By subtracting the total ice resistance obtained from the pre-sawn ice test from that of the level ice tests, the ice-breaking resistance can be extracted. Similarly, by subtracting the open water resistance from the pre-sawn ice resistance, the rotary submergence resistance of the ice can be determined. Therefore, the total ice resistance can be decomposed as follows:

$$R_{tot} = R_{br} + R_{pre} = R_c + R_b + R_{sub} + R_{open} \quad (1)$$

In the equation, R_c、R_b、R_{sub}、R_{open} represent the crushing force, bending failure force, rotary submergence resistance, and open water resistance, respectively.

Since the ship bow model is symmetrical about the centerline, theoretically, if the three segmented blocks collectively capture all force components during the ice-breaking process, the total ice resistance should be equal to twice the sum of the ice resistance measured by the three blocks. The total ice resistance can be expressed as:

$$R_{tot} = R_c + R_b + R_{sub} + R_{open} = 2(R_1 + R_2 + R_3) \quad (2)$$

In the equation, R_1, R_2, R_3 represent the ice resistance of the first block, the second block, and the third block, respectively.

TEST RESULTS AND DISCUSSIONS

Interaction Between Ship Bow and Ice

The ship-ice interaction process was observed through underwater video recordings, revealing a sequence of distinct stages. Initially, the ship's bow contacts with the ice sheet, leading to localized compressive failure in the central bow region. This results in compressive fractures, followed by the formation of circumferential cracks. Subsequently, the ice sheet is split into two parts by the bow wedge, forming independent ice segments that interact with the bow. In the next stage, these ice segments behave like cantilever beams, bending downward until they ultimately fracture. This bending failure induces longitudinal cracks on both the port and starboard sides of the ice sheet. As the model advances, the broken ice floes gradually move backward along the bow. A portion of the floes covers the bottom of the ship and continues to move further backward, while the remaining portion slides outward beneath the ice sheet on

both sides of the channel, as illustrated in Fig. 5.

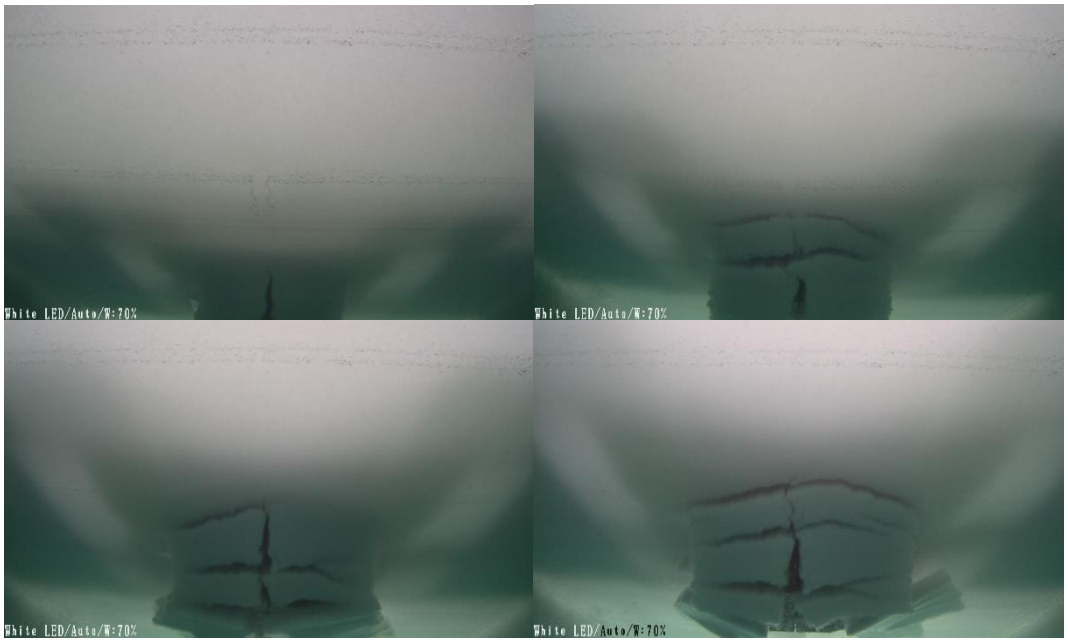

Figure 5 Ice-breaking process

From the pre-sawn ice test, the bow interacts with the pre-sawn ice sheet, causing the ice floes to rotate and submerge into the water. As the bow advances, the floes gradually move backward, forming a periodic process characterized by rotation, immersion, and sliding, as illustrated in Fig. 6. Only a small number of floes are further fragmented into smaller pieces. This process closely resembles the movement of broken ice floes observed during the breaking of level ice.

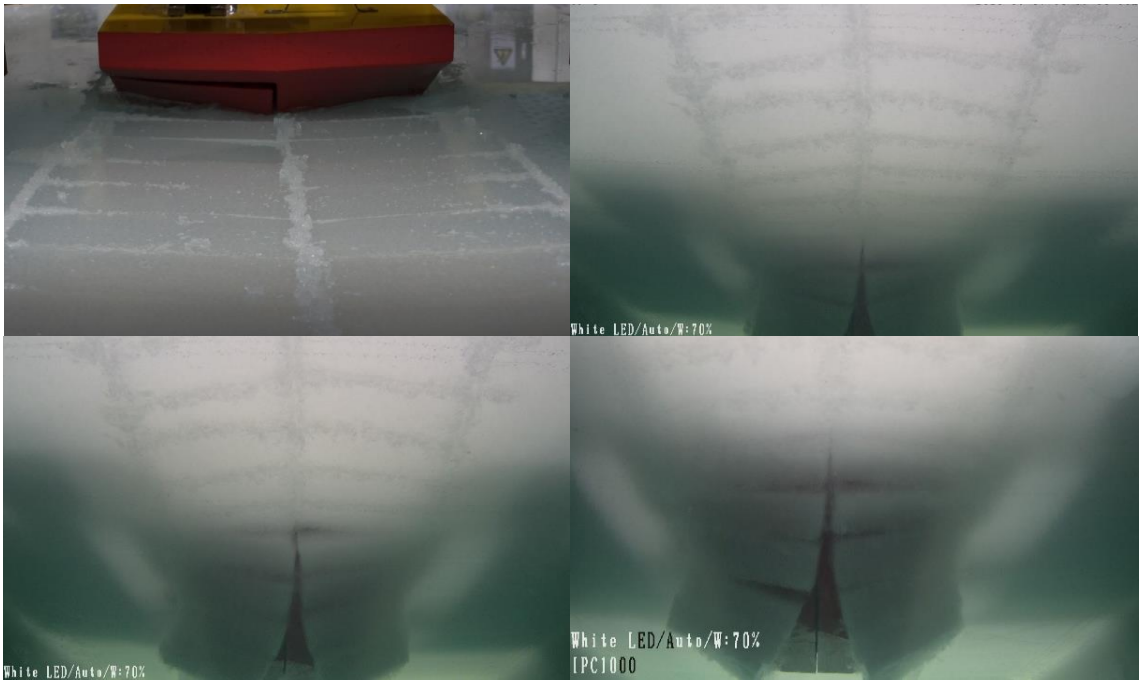

Figure 6 Stages of the pre-sawn ice test process

Component Analysis of Ice Resistance

The relationship between the total ice resistance and its components can be investigated by simultaneously measuring the total ice resistance of the model and the resistance of its segmented blocks using force sensors. The total ice resistance was measured at speeds of 0.01

m/s, 0.05 m/s, 0.10 m/s, 0.15 m/s, and 0.20 m/s, respectively.

A comparison among level ice resistance, pre-sawn icebreaking resistance, and open water resistance is illustrated in Fig. 7. It is evident that both the total ice resistance and its components increase with rising velocity. Furthermore, the proportion of the total ice resistance grows as the velocity increases, while the proportion of pre-sawn ice resistance gradually diminishes.

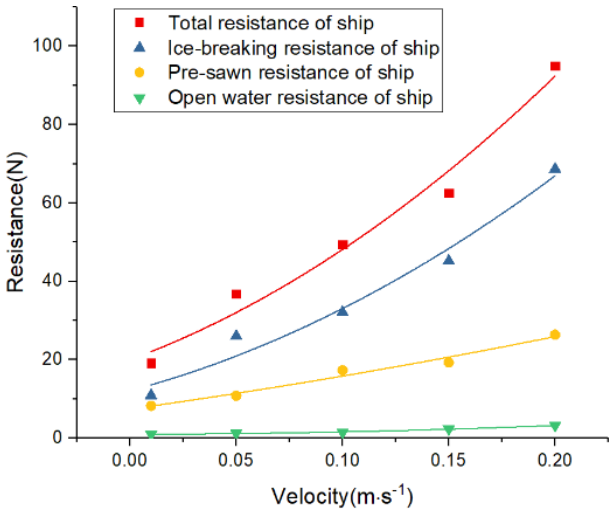

Figure 7 Comparison of the total ice resistance and its components

The average forces acting on the three segmented blocks were statistically analyzed. Under the level ice condition, the ice resistance of the first block accounts for more than 80% of the total ice resistance of the three blocks. Similarly, under the pre-sawn ice condition, the resistance of the first block constitutes over 73% of the total resistance of the blocks. Therefore, the first block is identified as the primary load-bearing segment. An analysis of the ice resistance of the first block as a function of ice-breaking speed is shown in Fig. 8. It is evident that, under both level ice and pre-sawn ice conditions, the ice resistance of the first block increases progressively with rising speed.

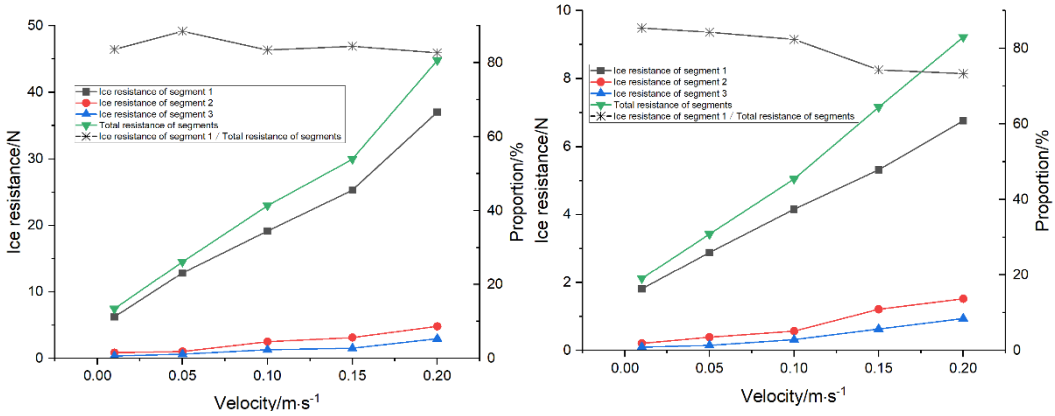

Figure 8 Comparison of different block resistance under level ice and pre-sawn ice condition

Given the symmetrical design of the bow model, and considering that the three force measurement segments were installed solely on the starboard side, the total ice resistance should theoretically be equivalent to twice the sum of the ice resistances measured by the three segments. To facilitate comparison, the ice resistance of segments 1 to 3 was multiplied by two and contrasted with the total ice resistance, as illustrated in Fig. 9. The discrepancy between the total ice resistance and the summed resistance of the segments is notably smaller under

level ice conditions compared to pre-sawn ice conditions. This difference may be attributed to factors such as ventilation phenomena and the splashing of water along the sides.

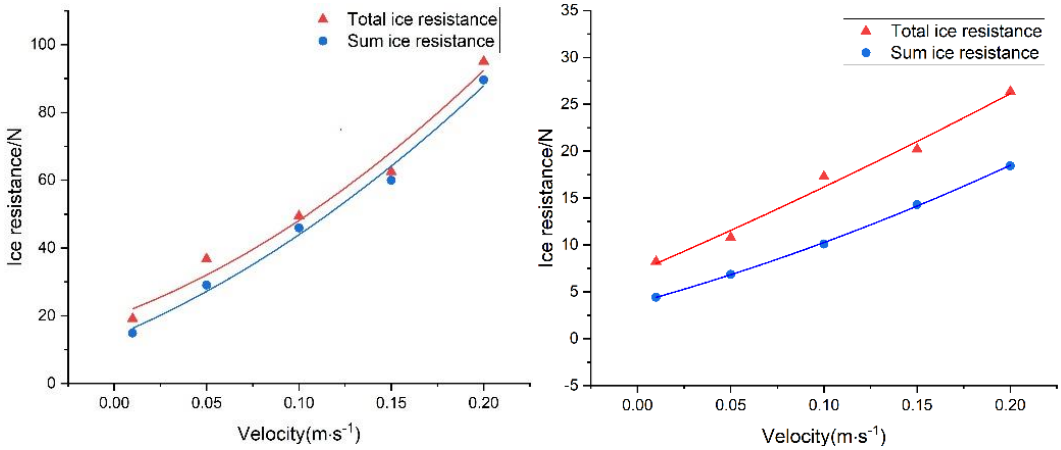

Figure 9 Comparison of total ice resistance with the sum of segments' resistance

DIMENSIONLESS ANALYSIS OF ICE RESISTANCE

Based on the test data, a dimensionless analysis method for ice resistance was employed to nondimensionalize each component of the ice resistance coefficients, thereby establishing an ice resistance prediction equation.

To extrapolate the prediction of ice resistance, the dimensionless analysis was applied to examine the correlation between ice resistance and ship form parameters (length L, draft T, and width B), ice conditions (ice thickness H, ice strength σ and ice density ρ), ice-breaking speed V, and gravitational acceleration g. The relevant parameters for each ice resistance component are derived by integrating the ice resistance components.

The ice-breaking resistance R_{Br}, which is influenced by ice strength, ice thickness, ice-breaking speed, and gravitational acceleration, can be expressed as $R_{Br} = k_1 f_1(\rho, B, V, \sigma, h)$, where k_1 is the ice-breaking resistance coefficient, denoted as C_{Br}.

The crushed ice resistance R_C can be expressed as $R_C = k_2 f_2(\rho, B, V, h)$, and k_2 is the coefficient of ice-breaking resistance caused by water flow, which is replaced by C_C.

The immersion resistance R_b is related to the subduction of crushed ice. Generally, the broken ice slides along the hull surface to the bottom of the hull so that the draft T parameter can be introduced, and the ice is affected by the buoyancy of the water, the ice resistance can be expressed as $R_B = k_3 f_3(\Delta\rho, B, g, h, T)$, and k_3 is the ice resistance coefficient caused by water buoyancy, which can be replaced by C_B.

To more accurately reflect the influence of ice characteristic parameters on the resistance components, two dimensionless parameters are introduced: the strength coefficient of the ship breaking ice and the Froude constant for the motion of the ice sheet.

The strength coefficient S_N, related to the ice-breaking speed and ice condition, can be expressed as $S_N = f_4(\rho, V, \sigma, h)$. The strength coefficient can be subsumed into the ice-breaking resistance, so the ice-breaking resistance can be expressed as $R_{Br} = S_N k_1 f_1(\rho, B, V, \sigma, h)$.

By using the formula of the Froude constant, the ship length is replaced by the thickness of ice, which can be expressed as $F_h = f_5(V, g, h)$. Therefore, the ice resistance induced by water flow can be expressed as $R_C = F_h k_2 f_2(\rho, B, V, g, h)$.

In summary, the ice-breaking resistance R_{Br} can be dimensionless as follows:

$$k_1 = \frac{R_{BR}}{f_1(\rho_i, B, h_i, V_M)} = C_{BR} = \frac{R_{BR}}{\rho_i B h_i V_M^2} \tag{3}$$

Where, C_{BR} is the ice-breaking resistance coefficient, ρ_i is ice density, B is ship width, h_i is ice thickness, V_M is ship velocity。

The crushed ice resistance R_C can be dimensionless as：

$$k_2 = \frac{R_C}{f_2(\rho_i, B, h_i, V_M)} = C_C = \frac{R_C}{\rho_i B h_i V_M^2} \tag{4}$$

Where, C_C is the coefficient of ice-breaking resistance caused by water flow.

The Immersion resistance R_B can be dimensionless as：

$$k_3 = \frac{R_B}{f_3(\Delta\rho_i, g, B, h_i, T)} = C_B = \frac{R_B}{\Delta\rho_i g B h_i T} \tag{5}$$

Where, C_B is the ice resistance coefficient caused by water buoyancy, $\Delta\rho_i$ is ice-water density difference.

The strength coefficients of ship-ice interactions can be dimensionless as follows.

$$S_N = f_4(\rho_i, B, V, \sigma_f, h_i) = \left[\frac{\rho_i B V_M^2}{\sigma_f h_i}\right]^{1/2} \tag{6}$$

Where, σ_f is the flexure strength of ice。

The ice thickness Froude number can be dimensionless as follows：

$$F_h = f_5(g, h, V_M) = \frac{V_M}{\sqrt{g h_i}} \tag{7}$$

The purpose of introducing two dimensionless parameters, the strength coefficient and the ice thickness Froude number, is to analyze the relationship between the ice-crushing resistance induced by water movement and the ice thickness Froude number, as well as to examine the relationship between the ice-breaking resistance and the mechanical properties of ice. Since the immersion resistance is independent of ice drift velocity and ice strength parameters, it is unnecessary to introduce additional parameters to express its correlation.

In the dimensionless analysis, the "ln-ln" expression method can be adopted to describe the aforementioned relationships. This approach is advantageous due to its ability to establish a perfect linear functional relationship, minimize the loss of original data, and provide results that align more closely with the measurements from model tests. The "ln-ln" relationship can be established as follows:

$$\ln C_c = a \ln F_h + b \tag{8}$$

$$\ln C_{Br} = c \ln S_N + d \tag{9}$$

In the equation, *a*, *b*, *c*, and *d* are correlation coefficients.

Therefore, the ice-breaking resistance coefficient and ice-breaking resistance coefficient can

be expressed as follows:

$$C_c = e^b F_h^{\ a} \tag{10}$$

$$C_{Br} = e^d S_N^c \tag{11}$$

Based on the above analysis, the ice resistance equation at any scale can be established, and the expression is as follows:

$$R_T = C_{BR}\rho_i B h_i V_M^2 + C_C \rho_i B h_i V_M^2 + C_B \Delta\rho_i g B h_i T + R_{OW} \tag{12}$$

$$R_T = e^d S_N^c \rho_i B h_i V_M^2 + e^b F_h^{\ a} \rho_i B h_i V_M^2 + C_B \Delta\rho_i g B h_i T + R_{OW} \tag{13}$$

Firstly, the test results can be reorganized and as listed in the following Table 2 and 3.

Table 2 Test results of level ice

V_M(m/s)	h_i(mm)	σ_f(kPa)	ρ(kg/m^3)	R_T(N)	R_{OW}(N)
0.01	40	50	916	19.12	0.32
0.05	40	50	916	36.83	0.53
0.1	40	50	916	49.45	0.63
0.15	40	50	916	62.49	0.92
0.2	40	50	916	95.01	1.12

Table 3 Test results of pre-sawn ice

V_M(m/s)	h_i(mm)	σ_f(kPa)	ρ(kg/m^3)	R_T(N)	R_{OW}(N)	R_B(N)+ R_C(N)
0.01	40	50	916	8.23	0.32	7.91
0.05	40	50	916	10.8	0.53	10.27
0.1	40	50	916	17.32	0.63	16.69
0.15	40	50	916	19.26	0.92	18.34
0.2	40	50	916	26.36	1.12	25.24

After the test results were sorted out, the above dimensionless analysis method was applied to obtain each resistance coefficient and the relationship between lnC_C and lnF_h、 lnC_{Br} and lnS_N, as listed in the following Table 4 and 5 and further depicted in Figure 9.

Table 4 The solution of lnC_C and lnF_h

V_M(m/s)	h_i(mm)	ρ(kg/m^3)	R_C(N)	C_C	F_h	lnC_C	lnF_h	C_B
0.01	40	916	0.42	249.193	0.01592	5.51822	-4.13998	0.00257
0.05	40	916	0.78	18.5114	0.07961	2.91839	-2.53054	0.00326
0.1	40	916	1.14	6.76381	0.15923	1.91158	-1.83739	0.00534
0.15	40	916	2.42	6.38145	0.23884	1.85339	-1.43193	0.00547
0.2	40	916	3.04	4.50920	0.31846	1.50612	-1.14424	0.00763

Table 5 The solution of lnS_N and lnC_{Br}

V_M(m/s)	h_i(mm)	ρ(kg/m^3)	R_B +R_C +R_{Br}(N)	S_N	lnS_N	R_{Br}（N）	C_{Br}	ln C_{Br}
0.01	40	916	18.8	0.16228	-1.81843	10.89	6461.22	8.77357
0.05	40	916	36.3	0.81140	-0.20899	26.03	617.761	6.42610
0.1	40	916	48.82	1.62280	0.48415	32.13	190.632	5.25034
0.15	40	916	62.57	2.43420	0.88962	44.23	116.632	4.75903
0.2	40	916	93.89	3.24561	1.17730	68.65	101.828	4.62328

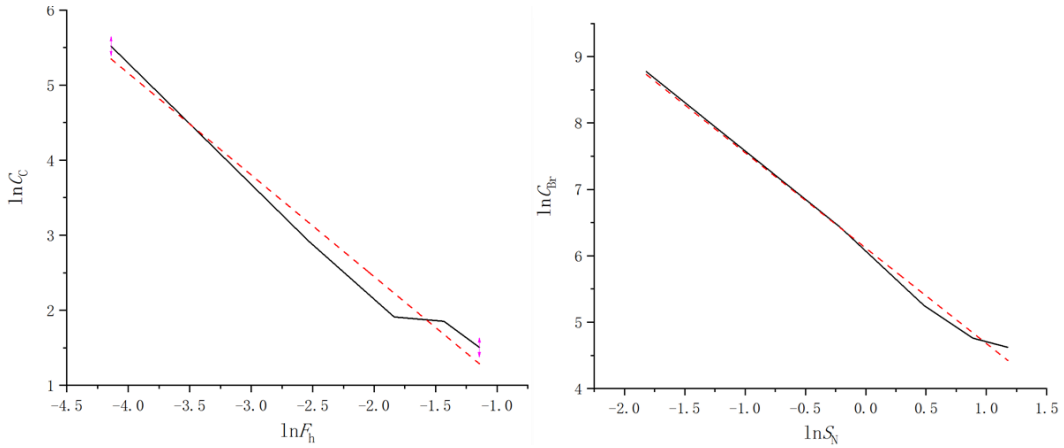

(1) $\ln C_C$ vs $\ln F_h$ (2) $\ln C_{Br}$ vs $\ln S_N$

Figure 9 Fitting of ln-ln expression results

Finally, the total ice resistance test prediction equation can be established as follows:

$$R_T = 453.5021 S_N^{-1.4372} \rho_i B h_i V_M^2 + 0.769588 F_h^{-1.3548} \rho_i B h_i V_M^2 + 0.004875 \Delta \rho_i g B h_i T + R_{OW} \quad (14)$$

DISCUSSION

In this study, a combination of segmented measurement of the ship's starboard resistance and the investigation of level ice, pre-sawn ice, and open water was employed to isolate the components of the hull's ice resistance and to derive the dimensionless coefficient of ice resistance. This approach effectively addressed the challenge associated with the level ice, pre-sawn ice, and open water method, where the ice-breaking processes of layered ice and pre-cut ice were typically disconnected. Consequently, this method facilitated clearer observations of how level ice breaking influences each resistance component.

However, due to constraints in the experimental setup, a fixed towing method was utilized for measuring the hull's ice resistance, which limited our ability to evaluate the effects of hull movement on ice resistance. This limitation may introduce some degree of influence on the experimental results. Total resistance was measured using a six-component force sensor, while three-component force sensors were employed to assess the resistance arising from segmented ice. This configuration provided valuable insights into the force dynamics acting on both the hull and its segments in various directions. Further analysis regarding the impact of hull movement on ice resistance will be conducted in subsequent research.

The relevant dimensionless method previously developed by Spencer was utilized to predict the ice resistance of R-Class icebreakers. This approach employed dimensionless analysis to explore the relationship between model-scale and full-scale performance metrics. By leveraging statistical and computational techniques, it assessed the resistance characteristics of both model and full-scale vessels under various operational scenarios. Building on this foundation, the current paper enhances the experimental methodology by directly measuring the individual resistance coefficients of the bow during the icebreaking process. This direct measurement minimizes errors associated with statistical data interpretation. Moreover, this refined approach better aligns with the contemporary requirements of the CSSRC's ice-water tank testing protocols.

CONCLUSIONS

This paper focuses on a typical ice-breaking bow for model testing and analytical research on ice breaking resistance. Direct measurements were conducted for the ice-breaking resistance

of the bow and its various ice resistance components. Additionally, a dimensionless analysis was performed on each resistance component to derive non-dimensional coefficients for ice resistance terms. The main conclusions are as follows:

1. The bow model was segmented to study the components of ice resistance, and the ice-breaking resistance of the bow was extracted. Underwater and surface videography techniques were employed to track and capture the entire process of bow-ice interaction, including contact, compression, bending failure, as well as the rotation, submersion, and sliding of broken ice. This provides technical reference for the mechanistic analysis of ship-ice interaction and the optimization of hull design.

2. The model test results indicate that the ice resistances experienced by the bow and its segments increase progressively with the ice-breaking speed. Furthermore, the ice-breaking speed has a certain influence on the ice-breaking mode of the bow. Analysis of the ice-breaking resistance components of the bow model reveals that the ice-breaking resistance constitutes a significant proportion, accounting for 50% to 70% of the total ice resistance. Moreover, the proportion of ice-breaking resistance gradually increases with higher ice-breaking speeds.

3. Research was conducted on the dimensionless analysis method for ice resistance components. A dimensionless expression method was established for each ice resistance term, taking into full consideration influencing factors such as hull parameters, ice conditions, mechanical properties of sea ice, and sailing speed. By introducing factors such as the strength coefficient for hull ice-breaking and the ice thickness Froude number, a dimensionless parametric equation for ice resistance was formulated.

ACKNOWLEDGEMENTS

The research sponsored by the National Key Research and Development Program (Nos. 2024YFC2816400, 2024YFC2816402) and National Natural Science Foundation of China (Grant No. G52192690, 52192694).

REFERENCES

[1]. Daniela Myland,Soren Ehlers. Influence of bow design on ice breaking resistance [J]. Ocean Engineering. 2016, 217-232.

[2]. ITTC, 2017. "Resistance Test in Ice," Recommended Procedures and Guidelines to the 28th ITTC.

[3]. ITTC, 2017. "Test Methods for Model Ice Properties," Recommended Procedures and Guidelines to the 28th ITTC.

[4]. Jeong S, Lee C, Cho S. Ice resistance prediction for standard icebreaker model ship [C]. Proceedings of the 20th International Offshore and Polar Engineering Conference. 2010, Beijing, China.

[5]. SPENCER D, JONES S J. Model-scale/full-scale correlation in open water and ice for Canadian Coast Guard "R-Class" icebreakers [J]. Journal of Ship Research, 2001, 45(4):249-261.

[6]. Valanto P. The Resistance of Ships in Level Ice[C]. SNAME Transactions, 2001, Vol.109, 2001, 53-83.

[7]. Yukui Tian, Yinghui Wang, Shaopeng Ji, etc. Design and Realization of CSSRC Small Ice Model Basin for Ice-related Fundamental Researches[C]. Port and Ocean Engineering under Arctic Conditions, June 9-13, 2019, Delft, Netherlands.

[8]. Yukui Tian, Shaopeng Ji, Xuan Zhang, etc. Experimental Analysis of Uniaxial Compressive Strength for Columnar Saline Model Ice[C]. Proceedings of the Twenty-eighth (2018) International Ocean and Polar Engineering Conference Sapporo, June 10-15, 2018, Japan.